



**POLITECNICO
MILANO 1863**

**Road and off-road vehicle design
Mechanical Engineering
Automotive and Motorsport Engineering, M.Sc.**

Assignments Summary

Group:

Pietro Nardon
Cristiano Riganti
Gianluca Meli

April 8, 2025

Contents

| | |
|---|----------|
| 1 Assignment 4: MacPherson LCA design | 1 |
| 1.1 Abstract | 1 |
| 1.2 Introduction | 1 |
| 1.3 Suspension's joints coordinates selection | 2 |
| 1.3.1 Objective and constraints | 2 |
| 1.3.2 Optimisation problem | 2 |
| 1.4 Internal forces computation | 5 |
| 1.5 Section pre-dimensioning and steering angle check | 9 |
| 1.6 FEM analysis and weight reduction | 12 |
| 1.6.1 Pre-dimensioning check | 12 |
| 1.6.2 Topology optimization with Altair Inspire | 13 |
| 1.6.3 Final FEM analysis | 14 |
| 1.7 Conclusions | 17 |
| 1.8 Manufacturing techniques | 17 |

1 Assignment 4: MacPherson LCA design

1.1 Abstract

The suspension of a road vehicle is a vital component in ensuring its best behaviour in terms of comfort and handling. In this assignment, the design of a MacPherson road vehicle suspension is treated, with a particular focus on the static assessment of the lower control arm.

The hard-points of the suspension were first calculated through a Matlab Sim-mechanics model and after that, a first design of the control arm has been developed considering the available room and kinematic requirements, after having performed a pre-dimensioning procedure. The control arm has then been optimized through the use of the *Altair Inspire* software, aiming to reduce its weight. As a last step, the lower control arm has been tested through a Finite Elements Method, by exploiting the *Dassault Systèmes Abaqus* software, to perform a static assessment on the final design with the given loads. The missing components of the suspension have been designed to produce a full scale drawing of the assembly, while a complete production drawing has been elaborated for the control arm only.

1.2 Introduction

The vehicle suspension should be designed to enhance comfort and ensure proper road holding capabilities. A large variety of road vehicles adopt the MacPherson suspension type, characterized by the presence of the lower control arm only and a spring-damper element in place of the upper control arm.

This kind of suspension design is really popular in the automotive industry because guarantees adequate performance at a relatively low cost and low space requirements, with respect to other solutions, such as the double wishbone suspension.

The considered suspension is the one of a front wheel of a front wheel drive vehicle.

The choice of the hard-points position has been performed through a 3D kinematic model developed in Matlab Sim-mechanics, with the objective of matching some target values of camber angle and toe angle during the wheel vertical travel. This choice has been discussed in detail in (Sec. 1.3).

Then an estimation of the suspension loads has been done and discussed in (Sec. 1.4), considering an extremely demanding and unlikely load condition, to have a high safety margin in the control arm dimensioning process.

The pre-design of the lower control arm is discussed in (Sec. 1.5), while its weight reduction and FEM analysis are discussed in (Sec. 1.6).

Finally, the drawings of the lower arm and the assembly have been developed through the use of the *Dassault Systèmes Catia V5* software.

1.3 Suspension's joints coordinates selection

Assuming that a dynamic study on the vehicle's performance was already carried out, it was requested to satisfy some kinematics objectives by choosing the coordinates of some particular suspension joints.

1.3.1 Objective and constraints

The kinematic objectives to be satisfied were regarding the camber angle and steering angle, which had to reach a determined value at different values of wheel travel. In particular, the angles were studied at the nominal position of the spring-damper assembly, at a full compression of 80 mm and at full extension of 95 mm, the objectives are reported in (Tab. 1).

| | Nominal | Compression | Extension |
|----------|-----------|-------------|-----------|
| Camber | -1° | -0°26'30" | -0°28'24" |
| Steering | -0°03'17" | -0°46'22" | -0°26'10" |

Table 1: Kinematic objectives

To reach these kinematic objectives the coordinates of some particular points were changed, respecting room constraints reported in (Tab. 2). The vehicle reference system is centred in a point inside the mean plane of the vehicle, with x axis pointing rearwards along the longitudinal direction, z is the vertical axis pointing upwards and y is created to make a right-handed reference system.

The studied points were:

- Point B : joint between wheel hub carrier and lower arm
- Point C_1 : joint between chassis and lower arm
- Point G : steering joint on the chassis

| | y [mm] | z [mm] |
|-------|-----------|-----------|
| B | 715 : 735 | -50 : -70 |
| C_1 | 390 : 410 | -45 : -65 |
| G | 300 : 320 | 86 |

Table 2: Room constrains

1.3.2 Optimisation problem

To reach the requested objectives, a optimization problem was set up, with the aim of reaching a good solution in a structured and precise way, using a limited amount of time and resources. It was decided to use a uniform grid approach, even if slow and not precise, due to its robustness and certainty of result.

The problem was set up as follows:

- Design variables: It was chosen to use as design variables all the varying joint coordinates pointed out in (Tab. 2). A `linspace` command was used in Matlab to create a vector of a certain number of elements for each design variable, using as limits (Tab. 2), subsequently they were combined and then inserted into the function to compute the requested angles.
- Angles computation: Using a provided SimMechanics model, steering and camber angle, at different compression lengths were computed, for each combination of design variable.

- Objective functions: After extracting the requested angles the objective functions for the optimisation method were computed. It was decided to use the mean square error of the computed angle respect to the target one, at each compression values, more precisely:

$$f_{camber} = \frac{(c_{nom} - c_{nom,t})^2 + (c_{compr} - c_{compr,t})^2 + (c_{exts} - c_{exts,t})^2}{3} \quad (1.1)$$

$$f_{steering} = \frac{(s_{nom} - s_{nom,t})^2 + (s_{compr} - s_{compr,t})^2 + (s_{exts} - s_{exts,t})^2}{3} \quad (1.2)$$

- Pareto front extraction: The objective functions were evaluated and an objective function domain was created. Inside the OF domain an optimization algorithm, containing the definition of a Pareto optimal condition, was run and a Pareto front extracted.

Due to the high number of possible combinations and long computational time, the simulation could only be run initially with a very coarse DV domain, leading to the results in (Fig. 1). Here it was evident the presence of at least one DV generating the clustering of the solutions in similar displaced areas of the domain, with a replicated trend. Even if the Pareto front was the optimal solution for this set of DV, the error values for each objective function were still very high, and the results were not acceptable.

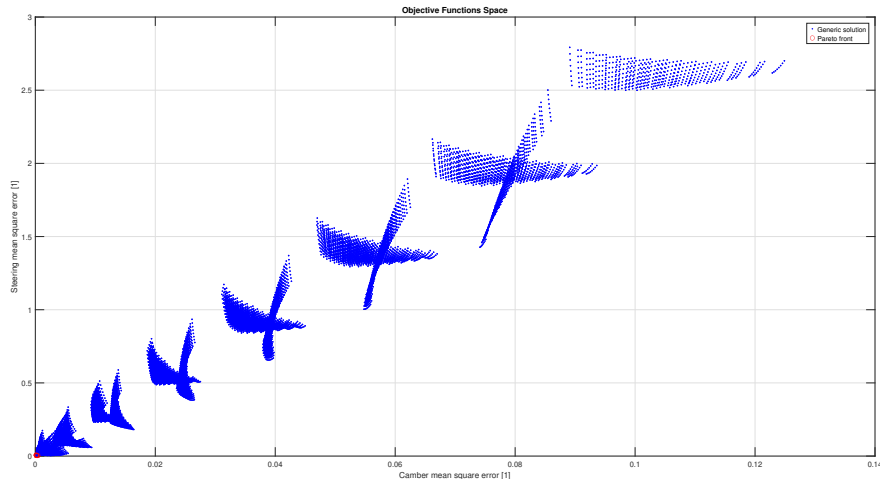


Figure 1: Coarse OF domain

Moreover, by analysing the DVs of the few Pareto solutions found, it could be noticed that they had three constant DVs, corresponding to one of their boundaries, thus could be excluded by the combinations by keeping them constant. Subsequent trials using this approach provided insufficient results again. This characteristic of the OF domain was found to be dependent on the discretisation of the DVs, which was very coarse.

Therefore other two simulations were launched, with a finer discretisation of the DVs. To avoid the running too computationally time demanding simulations, the number of elements in the linspace was kept low, but the boundary of each DV was reduced, centering it around the DVs that made the Pareto front of the first simulation in (Fig. 1). In this way it was possible to obtain a finer discretisation of the DVs domain, closer to the actual Pareto front.

This method proved to be successful, and within the Pareto Optimal solutions, the following was chosen (Tab. 3), which provided these results for steering and camber angle (Fig. 2). Here it is clear that each objective was satisfied.

| B_y | B_z | $C1,y$ | $C1,z$ | G |
|--------|--------|----------|--------|----------|
| 726 mm | -56 mm | 406.4 mm | -50 mm | 317.2 mm |

Table 3: Chosen joint coordinates

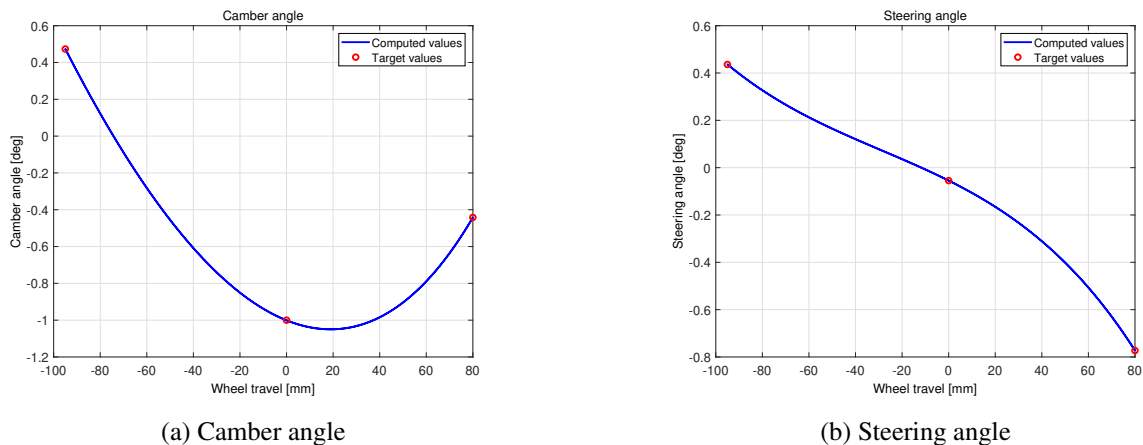


Figure 2: Optimisation results

The final coordinates necessary to build the suspension are reported in (Tab. 4)

| | x [mm] | y [mm] | z [mm] |
|-------|----------|----------|----------|
| A | 31.8 | 593 | 604 |
| B | -9.1 | 726 | -56 |
| C_1 | -10 | 406.4 | -50 |
| C_2 | 311 | 406.4 | -45.4 |
| D | -1.6 | 773.5 | -226.8 |
| E | -1.6 | 768.4 | 65.1 |
| F | 136.9 | 682.7 | 88.5 |
| G | 170 | 317.2 | 86 |
| O | 0 | 0 | 0 |

Table 4: Chosen joints coordinates

1.4 Internal forces computation

For the computation of the loads acting on the suspension system, three different contributions have been taken into account, corresponding to a vertical force (Z), a lateral one (Y) and a third longitudinal load (X). The three components are computed in (Eq. 1.3).

$$\begin{cases} Z = K F_{z,st} \\ Y = \mu_y Z \\ X = \mu_x Z \end{cases} \quad (1.3)$$

Where:

$$\begin{cases} F_{z,st} = g m_{s+u} = 9.81 \text{ m/s}^2 \cdot 390 \text{ kg} \simeq 3825 \text{ N} \\ K = 2.5 \\ \mu_y = 0.7 \\ \mu_x = 1.2 \end{cases}$$

Z is generated by a bump hit by the wheel and the factor K represents the dynamic effects on the load.

Y is generated during a turn and represents the cornering forces.

X can in general describe both accelerating or braking depending on the considered direction.

Note that our case study is an extreme one, in which a bump is hit during a turn, while braking/accelerating. All the resulting loads and stresses are thus sufficiently large to suppose a safe approach which is indeed exploited just for pre-dimensioning purposes. A more precise analysis should be performed for greater accuracy of the stresses (also with fatigue analysis and other kinds of assessment).

The main idea in computing the loads is that the arms of the suspension system are considered to be rods, meaning that they are capable of transmitting only axial forces. For this reason, the final goal is the computation of the in-plane components of the loads with respect to the control arm to be pre-dimensioned (represented by points B , C_1 and C_2).

The loads to be computed are represented in (Fig. 3).

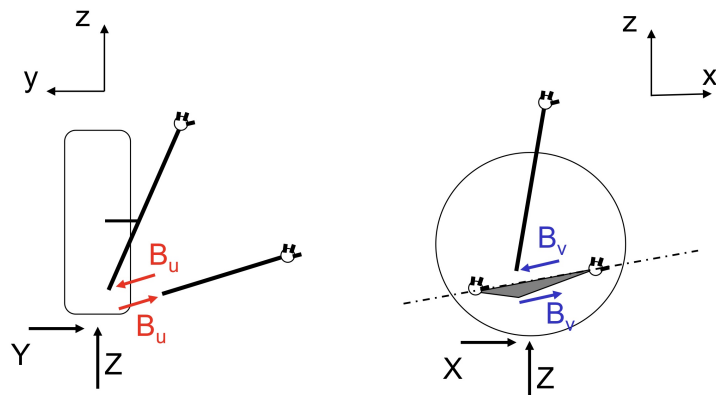


Figure 3: In-plane loads

Starting from the calculation of B_u , by exploiting the points summarized in (Tab. 4) and considering the scheme of (Fig. 4), the load is computed through a moment equilibrium about point A, as shown in (Eq. 1.4).

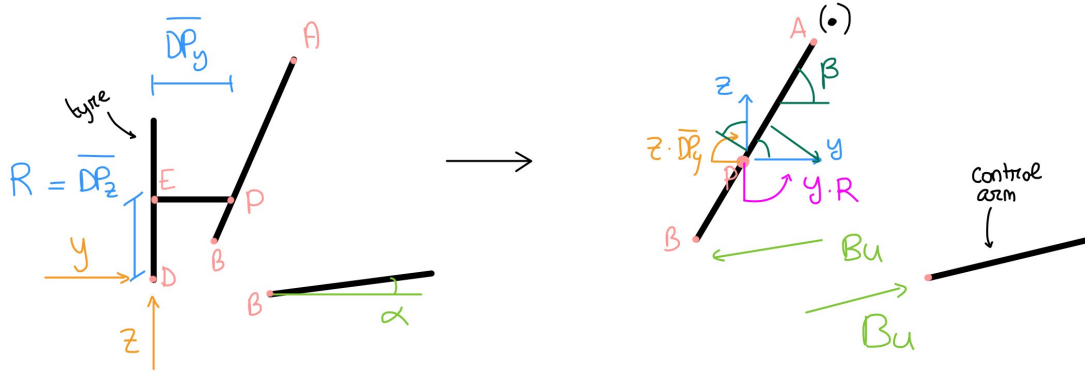


Figure 4: Structural scheme - YZ plane

$$Y \cdot R - Z \cdot \overline{DP_y} + (Y \cdot \sin \beta) \cdot \overline{AP_{yz}} - (Z \cdot \cos \beta) \cdot \overline{AP_{yz}} - B_u \sin(\beta - \alpha) \cdot \overline{AB_{yz}} = 0 \quad (1.4)$$

Where

$$\begin{cases} R = \overline{DP_z} = \overline{DE_z} = 291.9 \text{ mm} \\ \overline{DP_y} = \overline{AD_y} - \overline{AP_y} = 156.8 \text{ mm} \\ \overline{AP_y} = \overline{AP_z} \cdot \tan(90 - \beta) = 23.65 \text{ mm} \\ \overline{AP_z} = \overline{AE_z} = 538.9 \text{ mm} \\ \overline{AP_{yz}} = \sqrt{\overline{AP_y}^2 + \overline{AP_z}^2} = 539.4 \text{ mm} \\ \overline{AB_{yz}} = \sqrt{\overline{AB_y}^2 + \overline{AB_z}^2} = 673.3 \text{ mm} \\ \beta = \arctan \frac{\overline{AB_z}}{\overline{AB_y}} = 78.6 \text{ deg} \\ \alpha = \arctan \frac{\overline{BC_{1z}}}{\overline{BC_{1y}}} = 1.0755 \text{ deg} \end{cases}$$

Note that, being this a first tentative computation, the point C1 and C2 are considered to be at the same position in the YZ plane, for the computation of the angle α . Finally:

$$B_u = \frac{Y \cdot R - Z \cdot \overline{DP_y} + (Y \cdot \sin \beta - Z \cdot \cos \beta) \cdot \overline{AP_{yz}}}{\sin(\beta - \alpha) \cdot \overline{AB_{yz}}} = 5835 \text{ N} \quad (1.5)$$

With the same reasoning, the force B_v is also computed.

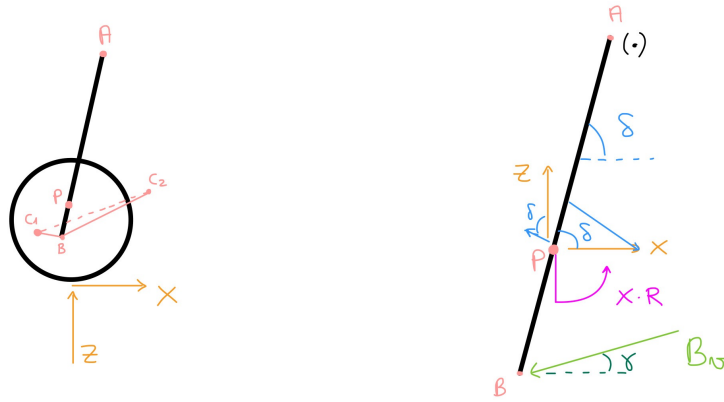


Figure 5: Structural scheme - XZ plane

Note that the braking condition is considered, being it the worst possible case due to the generation of a moment $X \cdot R$ coming from the brake caliper which is connected to the hub carrier, as a reaction to the braking action.

Also in this case, a moment equilibrium is performed about point A.

$$X \cdot R + (X \cdot \sin \delta) \cdot \overline{AP_{xz}} - (Z \cdot \cos \delta) \cdot \overline{AP_{xz}} - B_v \cdot \sin(\delta - \gamma) \cdot \overline{AB_{xz}} = 0 \quad (1.6)$$

Where

$$\begin{cases} \overline{AP_{xz}} = \sqrt{\overline{AP_x}^2 + \overline{AP_z}^2} = 593.9 \text{ mm} \\ \overline{AP_x} = \overline{AP_z} \cdot \tan(90 - \delta) = 33.35 \text{ mm} \\ \overline{AB_{xz}} = \sqrt{\overline{AB_x}^2 + \overline{AB_z}^2} = 661.3 \text{ mm} \\ \delta = \arctan \frac{\overline{AB_z}}{\overline{AB_x}} = 86.5 \text{ deg} \\ \gamma = \arctan \frac{\overline{C_1 C_2 z}}{\overline{C_1 C_2 x}} \end{cases}$$

Which, rearranging (Eq. 1.6), results in:

$$B_v = \frac{X \cdot R + (X \cdot \sin \delta - Z \cdot \cos \delta) \cdot \overline{AP_{xz}}}{\sin(\delta - \gamma) \cdot \overline{AB_{xz}}} = 13978 \text{ N} \quad (1.7)$$

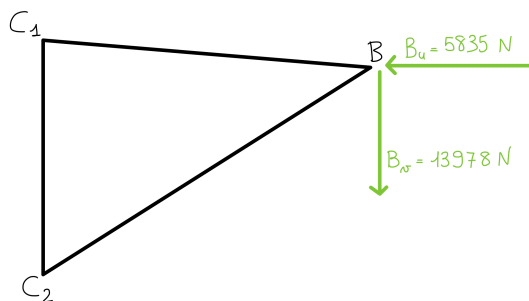


Figure 6: Final forces - Control Arm plane

Now, the focus turns to the computation of the reaction forces at the points C_1 and C_2 . At these locations, two different bushings are positioned, each one with proper stiffnesses. In particular, the two radial stiffnesses (the ones oriented as the force B_u) share the same value, while a correct ratio between the axial ones needs to be selected. The distribution of the reaction forces depends on this ratio. In principle any ratio could be chosen, but a possibility is to consider one stiffness much larger than the other, in order to approximate the constraints to a hinge (larger stiffness thus smaller compliance) and a roller (smaller stiffness thus larger compliance): for our analysis, this solution has been taken into account, so to obtain a statically determined structure which can be more easily reproduced also in both *Dassault Sistèmes Abaqus* and *Altair Inspire* softwares, as better explained in (Sec. 1.6).

The hinge has been positioned at point C_2 , the roller at point C_1 , has shown in (Fig. 7)

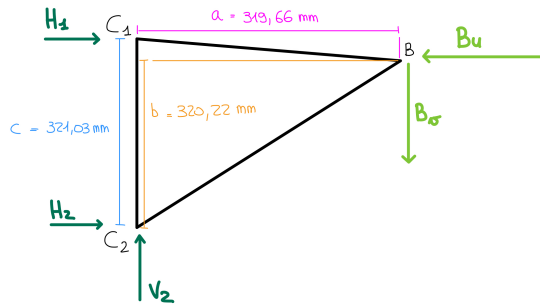


Figure 7: Reaction forces - Control Arm plane

The forces H_1 , H_2 and V_2 are computed through a system of three equations: horizontal forces equilibrium, vertical forces equilibrium, moment equilibrium about point C_2 (Eq. 1.8)

$$\begin{bmatrix} 1 & 1 & 0 \\ 0 & 0 & 1 \\ -c & 0 & 0 \end{bmatrix} \begin{bmatrix} H_1 \\ H_2 \\ V_2 \end{bmatrix} = \begin{bmatrix} B_u \\ B_v \\ B_v a - B_u b \end{bmatrix} \quad (1.8)$$

Which results in:

$$\begin{cases} H_1 = -8097 \text{ N} \\ H_2 = 13933 \text{ N} \\ V_2 = 13978 \text{ N} \end{cases}$$

1.5 Section pre-dimensioning and steering angle check

The first issue for the pre-dimensioning process is to define a first tentative shape of the control arm itself, which needs to ensure the correct functioning of all the required kinematics. In particular, the wheel must be able to perform a 37° steering angle inward and a 32° one outward at the nominal suspension position. The preliminary shape is shown in (Fig. 8).

The steering angles have been verified and shown in (Fig. 9).

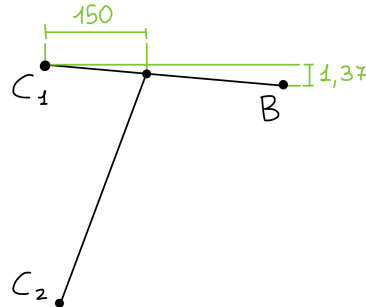


Figure 8: Schematic preliminary shape - Control Arm plane

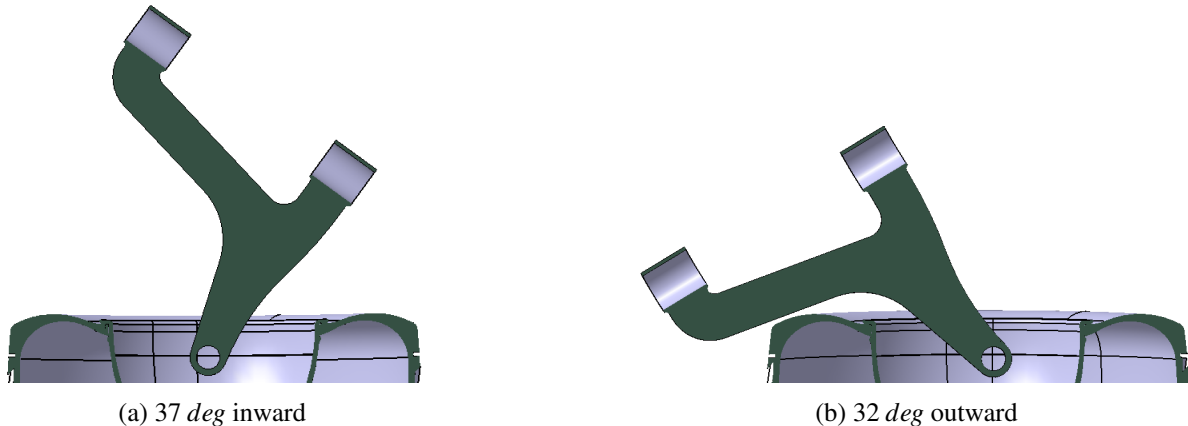


Figure 9: Steering angles check with a preliminary shape of the CA

To simplify the computation (always keeping in mind that we are referring to a first approximation solution), the structure is approximated as shown in (Fig. 10)

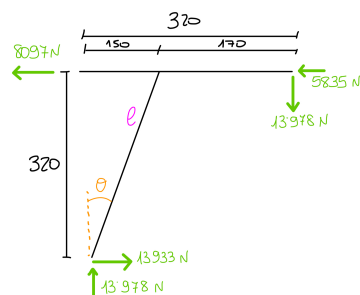


Figure 10: Schematic simplified shape - Control Arm plane

Considering that $l \approx 353.4 \text{ mm}$, $\theta \approx 25.11^\circ$ and the fact that the most stressed region is located where the two arms starting from C_1 and C_2 meet, the pre-dimensioning is performed with the following steps.

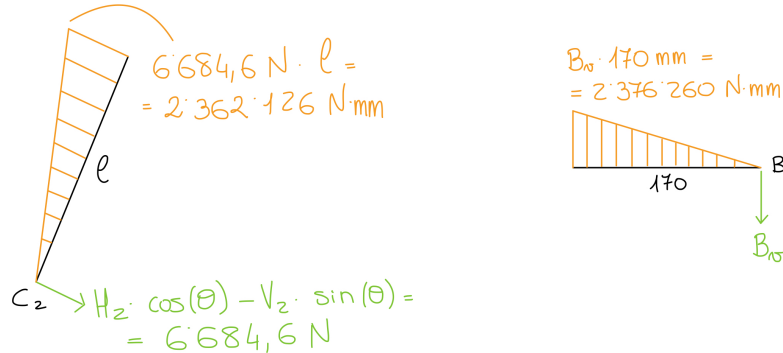


Figure 11: Bending moment diagrams (axial stresses are negligible)

At first, the maximum bending moment is computed:

$$M_b = 13978 \text{ N} \cdot 170 \text{ mm} = 2376260 \text{ N} \cdot \text{mm}$$

Then, a rectangular cross-section is considered, where the height is assumed to be one third of the base, as shown in (Fig. 12).

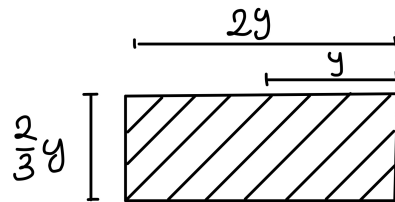


Figure 12: Cross-section

The cross-section moment of inertia is:

$$I = \frac{\frac{2}{3}y(2y)^3}{12} = \frac{4}{9}y^4$$

The maximum stress in the section is:

$$\sigma_{max} = \frac{M_b \cdot y}{I} = \frac{9M}{4y^3}$$

Considering 1.5 as safety coefficient (even if the considered load are already large) and selecting the *Aluminium A357 T6* as material (yielding stress $\sigma_y = 270 \text{ MPa}$):

$$\sigma_{max} \leq \frac{\sigma_y}{1.5}$$

$$y \geq \sqrt[3]{\frac{9 \cdot 1.5 \cdot M_b}{4 \cdot \sigma_y}} \simeq 30 \text{ mm}$$

Finally, the control arm cross-section results to be *60 mm* wide and *20 mm* large, as drawn in (Fig. 13), resulting in the geometry in (Fig. 14).

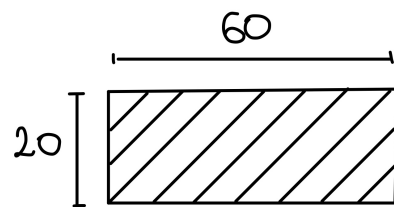


Figure 13: Final cross-section

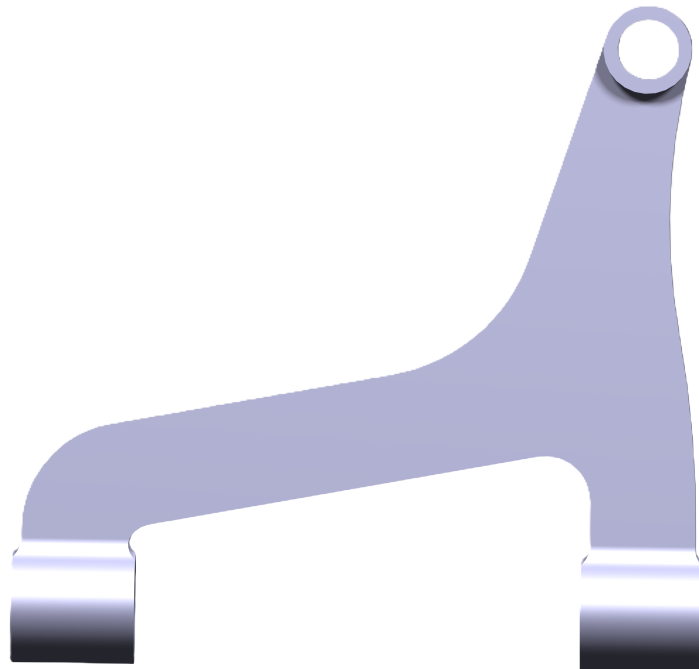


Figure 14: LCA predimensioning render

1.6 FEM analysis and weight reduction

After the pre-dimensioning phase, a first FEM analysis using *Dassault Sistèmes Abaqus* was carried out in order to verify that the stresses occurring in the LCA are below the yield stress limit of the material. After a satisfactory pre-dimensioning section was found, a structural optimisation analysis was carried out using *Altair Inspire*, with the aim of identifying regions where material could be removed, reducing the overall weight without affecting the overall stiffness of the component. In the end, a second, more thorough, FEM analysis was carried out to validate the design choices, using finer mesh and better elements.

1.6.1 Pre-dimensioning check

During the pre-dimensioning check phase, two different whole sections were analysed:

- The original section: $[60 \times 20] \text{ mm}^2$
- A smaller section: $[50 \times 16] \text{ mm}^2$

After analysing the original section it was clear that it was oversized and resulted in very low Von Mises stresses compared to the yield stress of the aluminium A357 T6. Therefore it was decided to reduce straight away the overall section of the LCA, still keeping the same ratio between length and width equal to 3, resulting in the second, smaller, section. Here the maximum Von Mises stress increased, lowering the safety factor η down to 1.44.

| | σ_{VM}^{max} | σ_{yield} | η |
|------------------|---------------------|------------------|--------|
| $[60 \times 20]$ | 118 MPa | 270 MPa | 2.29 |
| $[50 \times 16]$ | 188 MPa | 270 MPa | 1.44 |

Table 5: Pre-dimensioning results

As expected, the highest stresses were localised in two main regions: the region near the point C_2 , where the material has a very tight radius just close to the housing of the bushing, and in the curve where the piece of the arm coming from C_2 connects with the part that spans from B to C_1 .

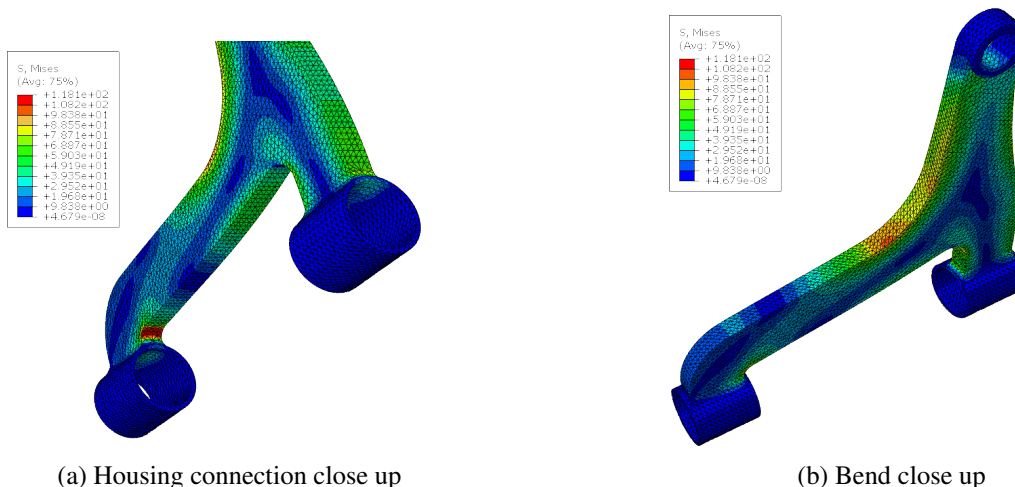


Figure 15: Close up of highly loaded regions for the 60 mm section

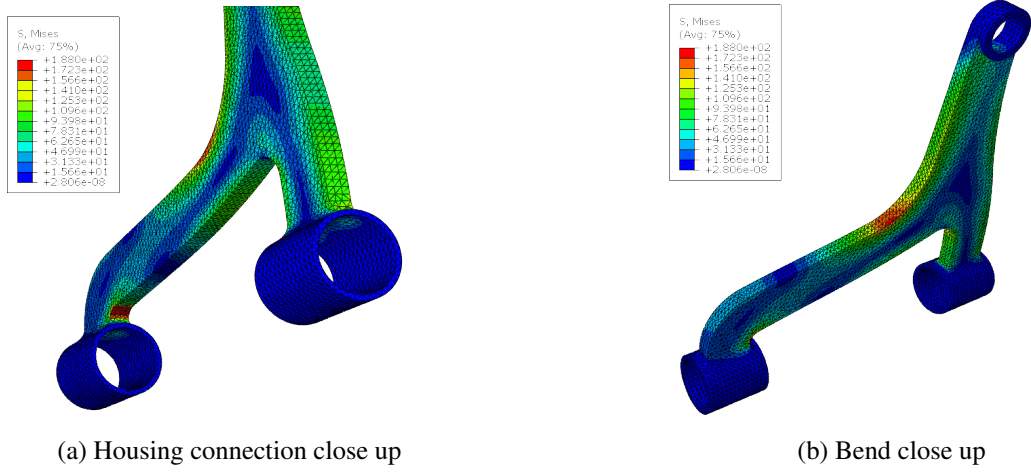


Figure 16: Close up of highly loaded regions for the 50mm section

1.6.2 Topology optimization with Altair Inspire

A topology optimization with the aim to reduce the LCA weight was run using *Altair Inspire*. The optimization was set up to maximise the stiffness of the LCA while reducing the mass of at least 50%, by removing material where not needed. The boundary conditions applied allowed the LCA to rotate along the bushing's axis, with the previously mentioned roller-hinge configuration.

The results shown in (Fig. 17) suggested that the central part of the LCA was lightly loaded, therefore the removal of material in that region would not affect considerably the overall stiffness. Other regions could be removed but, for safety reasons, it was decided not to excessively reduce the overall stiffness in an unnecessary way. Moreover, different runs inside *Altair Inspire* at different settings always suggested to remove the central part, independently of the material removal value. In addition, it was clear also from the *Abaqus* results that very low stresses characterised that region.

The LCA geometry was updated in *CatiaV5*, removing the aforementioned region.

The optimization resulted in a mass reduction from 1.52kg to 1.43kg, corresponding to a total removal of almost 0.1 kg or around 6 %, very important for handling performances.

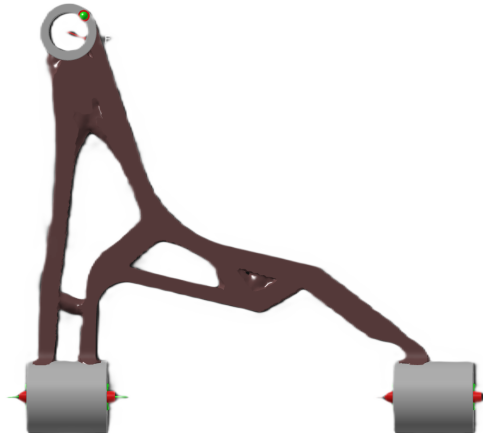


Figure 17: Optimization result using *Altair Inspire*

1.6.3 Final FEM analysis

After removing the unnecessary material another FEM analysis was carried out, which suggested that further modifications could be made to further reduce the material needed. It was decided to slightly change the LCA section shape, passing from the rectangular section of (Fig. 13) to an H-shaped one: after many iterations the chosen section was the one reported in (Fig. 18).

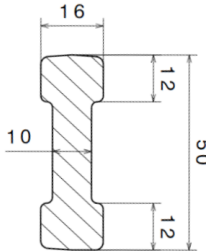


Figure 18: H-shaped section

The FEM analysis carried out with *Dassault Sistèmes Abaqus* with the following setup:

- Reference system: Centred in C_1 with the x axis passing through C_2 , y axis towards B and the z axis perpendicular to them.
- Material: Al A357 T6 with $\sigma_y = 270 \text{ MPa}$ and $\nu = 0.333$, mechanical elastic behaviour.
- Step: Static, linear perturbation
- Boundary conditions: Isostatic system with a realistic behaviour allowing the rotation around the bushing axis, the boundary condition was rigidly coupled to the entire internal cylinder holding the bushing or the ball joint.

| Point | BC | Dof |
|-------|---------|------------------|
| B | Support | All except U_z |
| C_1 | Roller | U_x, UR_x |
| C_2 | Hinge | UR_x |

Table 6: Boundary conditions

- External loads: The loads B_u and B_v computed in (Sec. 1.4), were applied to the B point, along the positive x and negative y direction respectively.
- Mesh: C3D20 twenty node tetrahedric element, with full integration, seed dimension of 5, with some local refinements in the most loaded and critical regions, such as the central bend and the connection of the bushing's housing.

The FEM analysis shows that the central part of the LCA, where the material was removed, was indeed lightly loaded, and the presence of a hole did not induce any stress-related issue in the region. Moreover, the LCA has particularly high Von Mises stresses along the bend (Fig. 20b) and in the corner where the LCA connects to the bushing representing the hinge connection (Fig. 20a). In the bend region the high stresses are due to the load B_v , which is particularly large along the x direction, while in the corner region the high concentration is due to the small radius and the presence of both radial and axial reaction forces.

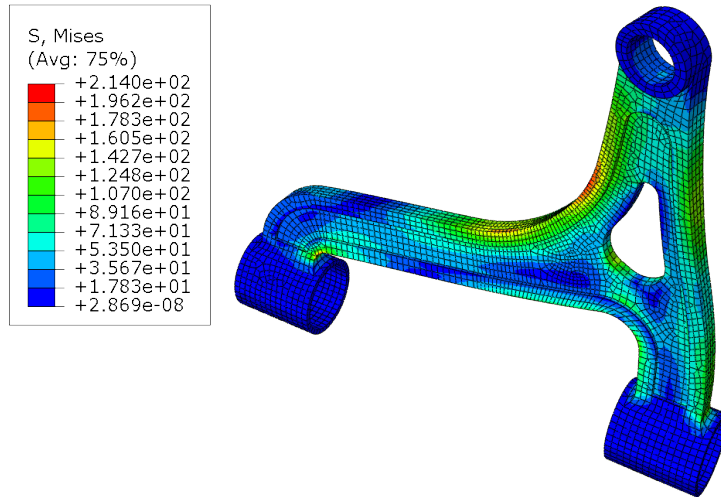


Figure 19: Von Mises stress

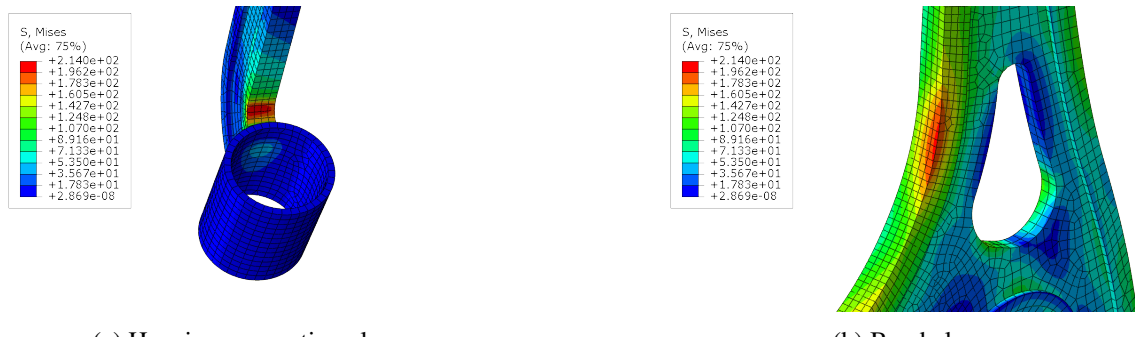


Figure 20: Close up of highly loaded regions

The safety coefficient was calculated using the maximum Von Mises stress computed by the software, which was equal to $\sigma_{VM}^{max} = 214 \text{ MPa}$:

$$\eta = \frac{\sigma_{yield}}{\sigma_{VM}^{max}} = \frac{270 \text{ MPa}}{214 \text{ MPa}} = 1.26 \quad (1.9)$$

Even if the safety coefficient is relatively low, the LCA results verified. Moreover, the safety coefficient achieved is close to the one used in (Sec. 1.5) to compute the initial section, even after all the modifications made in order to reduce the overall LCA weight. The load scenario applied of braking and hitting a bump while turning is highly unlikely and strongly demanding, therefore even if the safety coefficient is not particularly high, it can be regarded as an acceptable quantity, effectively passing the static load tests.

The final product, with all the needed features such as fillets and draft angles, is shown in (Fig. 21) and (Fig. 22).

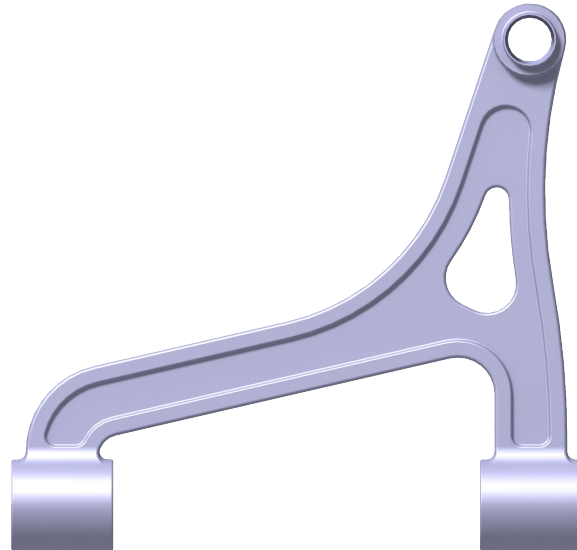


Figure 21: LCA Final render front view

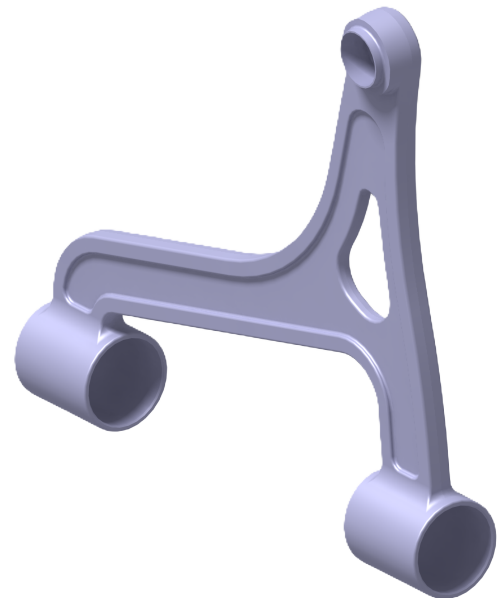


Figure 22: LCA Final render isometric view

1.7 Conclusions

In conclusion, the design and analysis process of the MacPherson lower control arm (LCA) has been carried out with a methodical approach, addressing both kinematic and structural requirements. The project started with the selection of suspension joints' coordinates aimed at ensuring optimal camber and steering angles across different wheel travel conditions. Subsequently it was possible to compute the internal forces to understand the loading conditions, leading to a well-informed pre-dimensioning phase.

The pre-dimensioning process provided a solid foundation for the FEM analysis, where different cross-sectional configurations were tested to ensure structural integrity while minimizing weight. The initial rectangular section, after many iterative simulations, was optimized in a H-shaped section that effectively balanced strength and mass reduction. The topology optimization performed with Altair Inspire further contributed to material reduction in non-critical areas, achieving a significant decrease in overall weight without compromising the mechanical performance.

The final FEM analysis confirmed that the optimized design meets the required performance criteria, with a safety factor of $\eta = 1.26$ and a maximum von Mises stress of 214 MPa , which is considered acceptable for the considered extreme loading scenario. The results validated the chosen material and design approach, proving that the LCA can withstand the applied forces while maintaining a lightweight structure.

However, further improvements could focus on refining the manufacturing process to enhance cost-efficiency and durability. Additionally, a fatigue analysis could be conducted to ensure long-term reliability under cyclic loading conditions. Exploring alternative materials with higher strength-to-weight ratios could also provide further weight reductions without compromising performance. Finally, real-world testing and validation would be beneficial to confirm the simulation results and to fine-tune the design based on empirical data.

Overall, this study demonstrates the effectiveness of an integrated design approach that combines kinematic optimization, structural analysis, and manufacturing feasibility, resulting in a well-balanced suspension component suitable for real-world applications.

1.8 Manufacturing techniques

In (Tab. 7) are reported the materials and production techniques chosen for the main components of the suspension. In particular, machining comprehends both turning and milling and is used to create the parts that must be in contact with some other components.

| Part | Material | Process |
|-------------|-----------|------------------------|
| Hub | Steel | Forging + Machining |
| Hub Carrier | Aluminium | Casting + Machining |
| Rim | Aluminium | Casting + Flow forming |
| Lower Arm | Aluminium | Casting + Machining |

Table 7: Production processes and materials